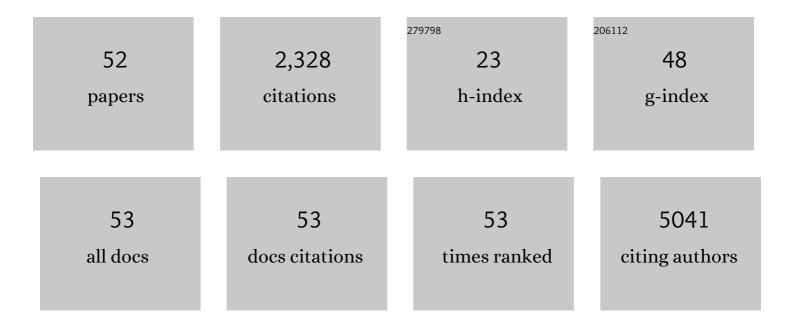
Changxi Zheng

List of Publications by Year in descending order

Source: https://exaly.com/author-pdf/5966888/publications.pdf Version: 2024-02-01



#	Article	IF	CITATIONS
1	Two-Dimensional CH ₃ NH ₃ PbI ₃ Perovskite: Synthesis and Optoelectronic Application. ACS Nano, 2016, 10, 3536-3542.	14.6	359
2	Helicity-Resolved Raman Scattering of MoS ₂ , MoSe ₂ , WS ₂ , and WSe ₂ Atomic Layers. Nano Letters, 2015, 15, 2526-2532.	9.1	241
3	Room temperature in-plane ferroelectricity in van der Waals In ₂ Se ₃ . Science Advances, 2018, 4, eaar7720.	10.3	224
4	Synthesis and Transfer of Large-Area Monolayer WS ₂ Crystals: Moving Toward the Recyclable Use of Sapphire Substrates. ACS Nano, 2015, 9, 6178-6187.	14.6	200
5	Strong Depletion in Hybrid Perovskite p–n Junctions Induced by Local Electronic Doping. Advanced Materials, 2018, 30, e1705792.	21.0	141
6	Quantification of ZnO Nanoparticle Uptake, Distribution, and Dissolution within Individual Human Macrophages. ACS Nano, 2013, 7, 10621-10635.	14.6	116
7	Strain Relaxation of Monolayer WS ₂ on Plastic Substrate. Advanced Functional Materials, 2016, 26, 8707-8714.	14.9	97
8	Acoustically-Driven Trion and Exciton Modulation in Piezoelectric Two-Dimensional MoS ₂ . Nano Letters, 2016, 16, 849-855.	9.1	91
9	Atomically thin lateral p–n junction photodetector with large effective detection area. 2D Materials, 2016, 3, 041001.	4.4	78
10	Direct Observation of 2D Electrostatics and Ohmic Contacts in Template-Grown Graphene/WS ₂ Heterostructures. ACS Nano, 2017, 11, 2785-2793.	14.6	74
11	Reversible Structural Swell–Shrink and Recoverable Optical Properties in Hybrid Inorganic–Organic Perovskite. ACS Nano, 2016, 10, 7031-7038.	14.6	68
12	Two-dimensional ferroelasticity in van der Waals β'-In2Se3. Nature Communications, 2021, 12, 3665.	12.8	53
13	Profound Effect of Substrate Hydroxylation and Hydration on Electronic and Optical Properties of Monolayer MoS ₂ . Nano Letters, 2015, 15, 3096-3102.	9.1	45
14	Capillary-bridge mediated assembly of aligned perovskite quantum dots for high-performance photodetectors. Journal of Materials Chemistry C, 2019, 7, 5954-5961.	5.5	41
15	Origin of Quantum Ring Formation During Droplet Epitaxy. Physical Review Letters, 2013, 111, 036102.	7.8	37
16	Caustic imaging of gallium droplets using mirror electron microscopy. Ultramicroscopy, 2011, 111, 356-363.	1.9	32
17	Reliable Synthesis of Largeâ€Area Monolayer WS ₂ Single Crystals, Films, and Heterostructures with Extraordinary Photoluminescence Induced by Water Intercalation. Advanced Optical Materials, 2018, 6, 1701347.	7.3	28
18	Disentangling the effects of doping, strain and disorder in monolayer WS ₂ by optical spectroscopy. 2D Materials, 2020, 7, 025008.	4.4	28

CHANGXI ZHENG

#	Article	IF	CITATIONS
19	Practical aspects of diffractive imaging using an atomic-scale coherent electron probe. Ultramicroscopy, 2016, 169, 107-121.	1.9	27
20	Roomâ€Temperature Singleâ€Photon Emission from Oxidized Tungsten Disulfide Multilayers. Advanced Optical Materials, 2017, 5, 1600939.	7.3	27
21	Laplacian image contrast in mirror electron microscopy. Proceedings of the Royal Society A: Mathematical, Physical and Engineering Sciences, 2010, 466, 2857-2874.	2.1	26
22	Electronic Band Structure of In-Plane Ferroelectric van der Waals β′-In ₂ Se ₃ . ACS Applied Electronic Materials, 2020, 2, 213-219.	4.3	26
23	Congruent evaporation temperature of GaAs(001) controlled by As flux. Applied Physics Letters, 2010, 97, .	3.3	24
24	Structure retrieval with fast electrons using segmented detectors. Physical Review B, 2016, 93, .	3.2	24
25	Synthesis of Ultrathin Composition Graded Doped Lateral WSe2/WS2Heterostructures. ACS Applied Materials & Interfaces, 2017, 9, 34204-34212.	8.0	22
26	Thickness and growth-condition dependence of in-situ mobility and carrier density of epitaxial thin-film Bi2Se3. Applied Physics Letters, 2014, 105, 173506.	3.3	18
27	Asymmetric coalescence of reactively wetting droplets. Applied Physics Letters, 2012, 100, .	3.3	15
28	Vertical Ge–Si Nanowires with Suspended Graphene Top Contacts as Dynamically Tunable Multispectral Photodetectors. ACS Photonics, 2019, 6, 735-742.	6.6	15
29	Three-Dimensional Chemical Mapping of a Single Protein in the Hydrated State with Atom Probe Tomography. Analytical Chemistry, 2020, 92, 5168-5177.	6.5	15
30	Grapheneâ€Enhanced 3D Chemical Mapping of Biological Specimens at Nearâ€Atomic Resolution. Advanced Functional Materials, 2018, 28, 1801439.	14.9	14
31	Ga droplet surface dynamics during Langmuir evaporation of GaAs. IBM Journal of Research and Development, 2011, 55, 10:1-10:7.	3.1	13
32	Direct Imaging of Liquid–Nanoparticle Interfaces with Atom Probe Tomography. Journal of Physical Chemistry C, 2020, 124, 19389-19395.	3.1	13
33	Addendum. Laplacian image contrast in mirror electron microscopy. Proceedings of the Royal Society A: Mathematical, Physical and Engineering Sciences, 2011, 467, 3332-3341.	2.1	11
34	Influence of bias voltage on morphology and structure of MgO thin films prepared by cathodic vacuum arc deposition. Surface and Coatings Technology, 2006, 201, 2387-2391.	4.8	10
35	Planar regions of GaAs (001) prepared by Ga droplet motion. Journal of Vacuum Science and Technology A: Vacuum, Surfaces and Films, 2016, 34, .	2.1	9
36	Nonlinear optical frequency mixing response of single and multilayer graphene. Optics Letters, 2016, 41, 1122.	3.3	9

CHANGXI ZHENG

#	Article	IF	CITATIONS
37	Influence of\$hboxO_2\$Flow Rate on Structure and Properties of\$hboxMgO_x\$Films Prepared by Cathodic-Vacuum-Arc Ion Deposition System. IEEE Transactions on Plasma Science, 2006, 34, 1099-1104.	1.3	8
38	Controlled graphene encapsulation: a nanoscale shield for characterising single bacterial cells in liquid. Nanotechnology, 2018, 29, 365705.	2.6	8
39	Large-scale process optimization for focused ion beam 3-D nanofabrication. International Journal of Advanced Manufacturing Technology, 2013, 64, 587-600.	3.0	7
40	Multidimensional analysis of excitonic spectra of monolayers of tungsten disulphide: toward computer-aided identification of structural and environmental perturbations of 2D materials. Machine Learning: Science and Technology, 2021, 2, 025021.	5.0	7
41	Annealing effect of thermal spike in MgO thin film prepared by cathodic vacuum arc deposition. Materials Chemistry and Physics, 2013, 143, 209-212.	4.0	6
42	Novel GaAs surface phases via direct control of chemical potential. Physical Review B, 2016, 93, .	3.2	5
43	Quantification of evaporation induced error in atom probe tomography using molecular dynamics simulation. Ultramicroscopy, 2017, 182, 28-35.	1.9	5
44	Influences of arc current on composition and properties of MgO thin films prepared by cathodic vacuum arc deposition. Materials Chemistry and Physics, 2010, 124, 1146-1150.	4.0	2
45	In situ monitoring of resistivity and carrier concentration during molecular beam epitaxy of topological insulator Bi ₂ Se ₃ . Proceedings of SPIE, 2013, , .	0.8	2
46	Electron caustic lithography. AIP Advances, 2012, 2, .	1.3	1
47	Facilitating Quantitative Analysis of Atomic Scale 4D STEM Datasets. Microscopy and Microanalysis, 2016, 22, 474-475.	0.4	1
48	Corrections to "Influence of O2Flow Rate on Structure and Properties of MgOxFilms Prepared by Cathodic-Vacuum-Arc Ion Deposition System". IEEE Transactions on Plasma Science, 2007, 35, 518-518.	1.3	0
49	Relief of surface stress at steps during displacive adsorption of As on Si(111). Applied Physics Letters, 2012, 100, 201602.	3.3	0
50	Nanoindentation on Graphene Encapsulated Single Cells. Microscopy and Microanalysis, 2017, 23, 744-745.	0.4	0
51	SIMULATION OF MIRROR ELECTRON MICROSCOPY CAUSTIC IMAGES IN THREE-DIMENSIONS. Surface Review and Letters, 2018, 25, 1950013.	1.1	0
52	Mass spectrometry inside single proteins by atom probe tomography. Microscopy and Microanalysis, 2019, 25, 334-335.	0.4	0